energies

MDPI

Article

Energy Savings Resulting from Using a Near-Surface Earth-to-Air Heat Exchanger for Precooling in Hot Desert Climates

Ali Pakari * and Saud Ghani

Department of Mechanical and Industrial Engineering, College of Engineering, Qatar University, Doha P.O. Box 2713, Qatar; s.ghani@qu.edu.qa
* Correspondence: ali.pakari@qu.edu.qa

Abstract: Given the substantial energy use for space cooling in buildings, integrating energy-efficient and sustainable cooling systems into buildings has become increasingly more important. Even though the cooling potential of a near-surface earth-to-air heat exchanger (EAHE) with grass cover was demonstrated in previous studies, the energy savings and environmental benefits resulting from using the EAHE have not yet been quantified. Therefore, in this study, we quantify the energy savings resulting from using a near-surface earth-to-air heat exchanger (EAHE) with grass-covered ground as a precooling unit in hot desert climates. The outlet air conditions of the EAHE during 9 months of the year (March to November), where space cooling is required, are predicted using a 3D transient CFD model, which is validated against field measurements. The EAHE is fabricated from a 1 mm thick aluminum tube with a diameter of 0.15 m and a length of 21.5 m, buried 0.4 m deep. The results showed that the EAHE can cool ambient air by up to 8.5 °C at an air flow rate of 607 m^3/h, corresponding to a cooling capacity of 1700 W and a COP of 17. The daily average cooling capacity of the EAHE is about 560 W for an average operation period of 15.1 h per day. When used as a precooling unit for conventional cooling systems, the highest estimated monthly energy savings is 115 kWh, and the estimated annual savings is 741 kWh.

Keywords: energy savings; electricity savings; precooling; ground cooling; computational fluid dynamics (CFD); transient simulations

Citation: Pakari, A.; Ghani, S. Energy Savings Resulting from Using a Near-Surface Earth-to-Air Heat Exchanger for Precooling in Hot Desert Climates. *Energies* **2021**, *14*, 8044. https://doi.org/10.3390/en14238044

Academic Editors: Francisco P. Brito and Gianpiero Colangelo

Received: 12 October 2021
Accepted: 29 November 2021
Published: 1 December 2021

1. Introduction

The built environment accounts for a considerable portion of the worldwide energy use and greenhouse gas emissions, with a significant increase every year [1]. For example, between 1990 and 2016, the worldwide energy consumption for space cooling in buildings more than tripled [2]. Of the total electricity use in buildings, cooling accounts for approximately 15% in the United States [3] and 19% in the world [2]. Given the substantial contribution of space cooling in buildings to global energy consumption, integrating energy-efficient and sustainable cooling systems into buildings has become increasingly more important.

In hot desert climates, one energy-efficient approach is using the ground as a heat sink to lower the ambient air temperature for space cooling [4,5]. The soil temperature at a considerable depth, a few meters, is substantially different from the ambient air and is nearly equal to the mean annual ambient air temperature [6]. Therefore, in ground cooling systems, ambient air is passed through tubes buried under the ground, where heat transfer occurs between the soil and the air in the tubes, and according to the season and time of the day, the air temperature could increase (during winter) or decrease (during summer) [7,8]. A number of recent studies have investigated ambient air cooling using earth-to-air heat exchangers (EAHE), including numerical [9–12] and experimental examples [13–16], with the burial depth of the EAHE ranging from 1.5 to 5 m.

In a numerical study by Wei et al. [9], the performance of a buoyancy-driven EAHE was investigated when employed in a building located in Chongqing, China. The EAHE

was 40 m long and 0.5 m in diameter and buried 4 m deep. It was estimated that the maximum daily cooling capacity of the EAHE was 56.3 kWh, while the maximum heating capacity was 111.1 kWh. Wang et al. [10] developed a regression model to predict the outlet temperature of an EAHE used in livestock building. CFD simulations and statistical techniques were used to develop the regression model. A depth of 2 m was selected for the EAHE. The effect of various operational and geometrical parameters on the performance of the EAHE was investigated using the developed model. Congedo et al. [11] investigated the use of an EAHE coupled with an air-source heat pump in a building located in Turin, Italy. The performance of the EAHE was modeled using TRNSYS 17 for multiple lengths, flow rates, and soil types. The results showed that coupling the EAHE to the air-source heat pump improved its performance. In a study by Zhou et al. [12], the performance of an EAHE integrated with phase change material was investigated using a 3D CFD model. The operational conditions of the simulations corresponded to Chongqing, China. The results showed that integrating the phase change material to the EAHE improved its cooling performance. On average, the air temperature was cooled by an extra 1.67 °C.

In an experimental study, Vaz et al. [13] investigated the thermal potential of using an EAHE in the south of Brazil. The results showed that the best heating performance was obtained in February, while the best cooling performance was obtained in May. Sakhri et al. [14] investigated the performance of an EAHE that was 66 m in length, 0.11 m in diameter, and buried 1.5 m deep. No fan was connected to the EAHE, which was installed in the southwest of Algeria. The results showed that the performance of the EAHE was strongly dependent on the weather conditions. In an experimental study, Hsu et al. [15] investigated the performance of an EAHE connected to a cafeteria building in Nantou, Taiwan. The EAHE included seven parallel tubes 50 m in length, 0.25 m in diameter, and 3.5 in depth. It was reported that using an EAHE is feasible for providing thermal comfort with the annual COP reaching 27.2. Díaz-Hernández et al. [16] experimentally investigated the performance of an EAHE in Mexico from August to January. The EAHE was 6 m in length and about 0.1 in diameter and was buried at a depth of 2.5 m. The results showed that the best cooling performance of the EAHE was in August, while the best heating performance was in January.

Li et al. [17] experimentally investigated the ventilation and cooling performance of a combined solar chimney and EAHE, which consisted of a 30 m long PVC pipe with a diameter of 0.3 m buried at 3 m deep. Using the EAHE, the ambient air temperature was lowered by about 12.5 °C corresponding to a cooling capacity of about 1398 W. In an experimental study by Wei et al. [18], an EAHE system, consisting of a 40 m long PVC pipe 0.16 in diameter and buried 3 m deep, was integrated to a building to provide space cooling and heating. It was shown the EAHE can lower the outdoor air temperature by about 9.1 °C in cooling mode and increase the outdoor air temperature by about 5.5 °C in heating mode. It was concluded that integrating the EAHE to a building would reduce its cooling load by 55.4 W/m^2 and reduce its heating load by 40.4 W/m^2. The maximum cooling capacity of the EAHE was about 1273 W, while the average was about 774 W.

In these studies, considerable cooling potential was demonstrated; however, due to the complexity and high initial cost of burying tubes at a great depth, it is not economical to use deep buried EAHE for small cooling systems, for example, in residential buildings.

The topsoil layer of a bare or exposed ground gets heated to temperatures significantly higher than the ambient air temperature [19], mainly due to the incident solar radiation. While the topsoil temperature of a ground with vegetation or plant cover is substantially lower than that of a bare ground [20,21]. By lowering evaporation from the top layer of the soil, the vegetation cover prevents the soil temperature from becoming higher than that of the ambient air.

A near-surface EAHE with vegetation or plant ground cover is a system that enables cooling the ambient air temperature without the need to bury the system deep below the ground surface [22]. In this approach, heat is rejected from the hot ambient air pass-

ing through the EAHE tubes to the relatively cooler topsoil, therefore simplifying the installation and lowering the initial cost.

It was shown in previous studies that using the near-surface EAHE for space cooling can save energy and protect the environment; however, the energy savings and environmental benefits resulting from using the EAHE have not yet been quantified. Therefore, the objective of this study is to quantify the energy savings resulting from using a near-surface EAHE with grass-covered ground as a precooling unit in Doha, Qatar, which has a hot desert climate according to the Köppen climate classification. The performance of the EAHE during 9 months of the year (March to November) was predicted using three-dimensional (3D) transient computational fluid dynamics (CFD) simulations. The boundary conditions of the simulations were defined according to measured air temperature, relative humidity, and soil temperatures at various depths during the year. The CFD model was validated against experimental measurements of a near-surface EAHE.

The remainder of this paper is structured as follows. The experimental setup is outlined in Section 2.1. Section 2.2 presents the details of the CFD simulations. In Section 3, the results are presented and discussed. The main conclusions of this study are listed in Section 4.

2. Methods

2.1. Experiments

The EAHE was fabricated from a 1 mm thick aluminum tube with a diameter of 0.15 m (6 in) and a total length of 21.5 m. The burial depth of the tube was 0.4 m (Figure 1a). As shown in Figure 1b, a 100 W fan was used to drive air through the EAHE. The fan power was determined from the specifications as provided by the manufacturer.

During April and May 2019, the EAHE was tested in the Aspire turf development farm in Doha, Qatar. The ground was covered with short grass, and the soil was a mixture of 90% sand and 10% compost. During the experiments, the EAHE was run continuously 24 h a day. As shown in Figure 1c,d, the temperature of the air entering and leaving and along the EAHE was measured by means of data loggers (Temperature and Humidity Data Logger, iButtonLink). The temperature measurements were recorded every 10 min with an accuracy of ± 0.5 °C. The average air velocity through the EAHE was measured using a hot wire probe (velocity probe 0635 1535, Testo) with an accuracy of ± 0.03 m/s. The average air velocity was 9.24 m/s, which corresponded to a flow rate of 607 m^3/h. More details about the experiments can be found in [22].

The cooling capacity, P_{cooling}, of the EAHE is determined by the following equation:

$$P_{\text{cooling}} = \rho V C_p (T_{\text{in}} - T_{\text{out}}) \quad (1)$$

where ρ (1.13 kg/m^3) is the density of air, V (0.169 m^3/s) is the air volume flow rate, C_p (1047 J/kg K) is the specific heat of air, T_{in} is the inlet air temperature, and T_{out} is the outlet air temperature.

The coefficient of performance (COP) of the EAHE is determined using the following equation:

$$\text{COP} = \frac{P_{cooling}}{P_{\text{fan}}} \quad (2)$$

where P_{fan} (W) is the EAHE fan power.

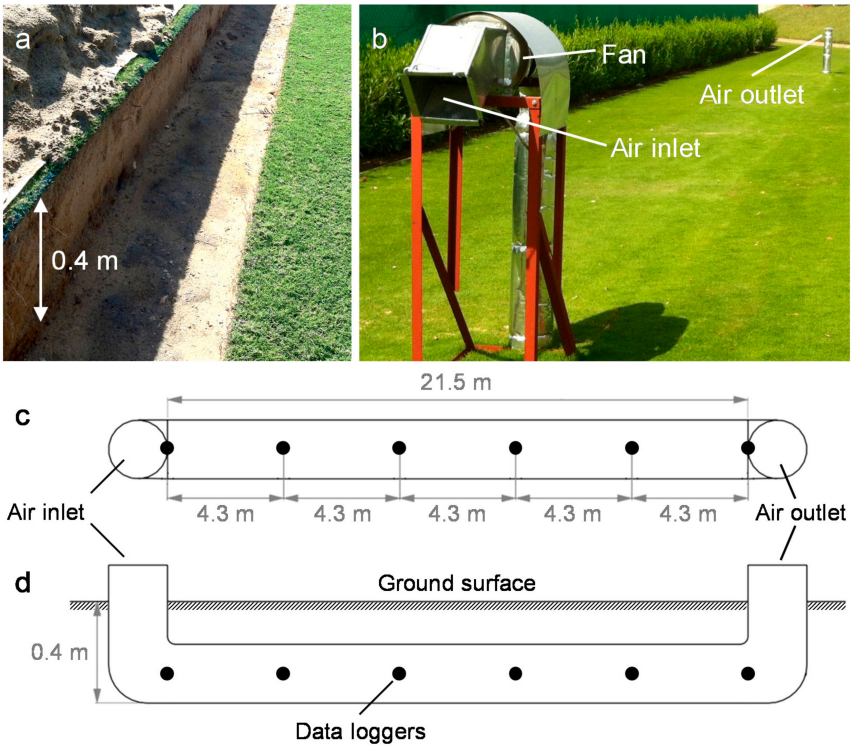

Figure 1. (**a**) Picture of the trench where the EAHE tube was buried. (**b**) Picture of the assembled EAHE. (**c**) Schematics of the top view and (**d**) side view of the EAHE showing the measurement configuration.

2.2. CFD Model

The commercial CFD code Ansys Fluent 18 was used to model the EAHE. The solved equations to predict the EAHE outlet air conditions include the 3D unsteady Reynolds-averaged Navier–Stokes (RANS) equations, energy conservation equation, and species conservation equation. The standard k–ε turbulence model was used for closure. The following assumptions are made to simplify the governing equations. The soil and tube thermal conductivity and heat capacity are isotropic and constant.

The SIMPLE algorithm was used for pressure–velocity coupling. Second-order discretization was used for all the terms in the governing equations. The iterations were stopped, and convergence was assumed to be reached when all the scaled residuals, as defined in the Ansys Fluent 18 user guide, have leveled off and reached a minimum value of 10^{-5} for x, y, and z velocity; 10^{-4} for continuity, k, and ε; and 10^{-6} for energy and species.

2.2.1. Computational Domain and Boundary Conditions

The domain consisted of two parts, the soil block and the air inside the EAHE tube (Figure 2), while the thin layer of the aluminum tube was modeled using the shell conduction model. For the tube walls, the standard wall functions by Launder and Spalding [23] were used. As shown in Figure 2a,b, the distance between the tube and the outer boundaries of the soil block, 0.5 m, was selected according to experimental results of a previous study [22], since it was shown that the temperature of the soil at this distance is not affected by the heat transfer from the EAHE. Measured dry-bulb air temperature, relative humidity, and soil temperature at various depths during the day were inputs to the model. The temperatures of the side boundaries of the soil block were set to change with time and depth according to measured soil temperatures at depths of 55, 140, 225, and 320 mm; no further variation in soil temperature was considered after a depth of 320 mm. The top boundary of the soil block represented a distance of 55 mm under the ground, and its temperature was set using measured soil data. On the other hand, the temperature of the bottom boundary of the soil block was set using temperature measurements at a depth of 320 mm. A uniform

thermal conductivity of 1.5 W/m K was assumed for the soil. The density and specific heat of the soil were set to 1742 kg/m^3 and 1175 J/kg K, respectively [24]. The material properties of the EAHE tube were set as follows: density of 2719 kg/m^3, specific heat of 871 J/kg K, and thermal conductivity of 202.4 W/m K. The inlet boundary of the EAHE was set as a velocity inlet (9.24 m/s), and at the outlet, zero static gauge pressure was applied. To match the field measurements, a time step of 10 min was selected for the simulations.

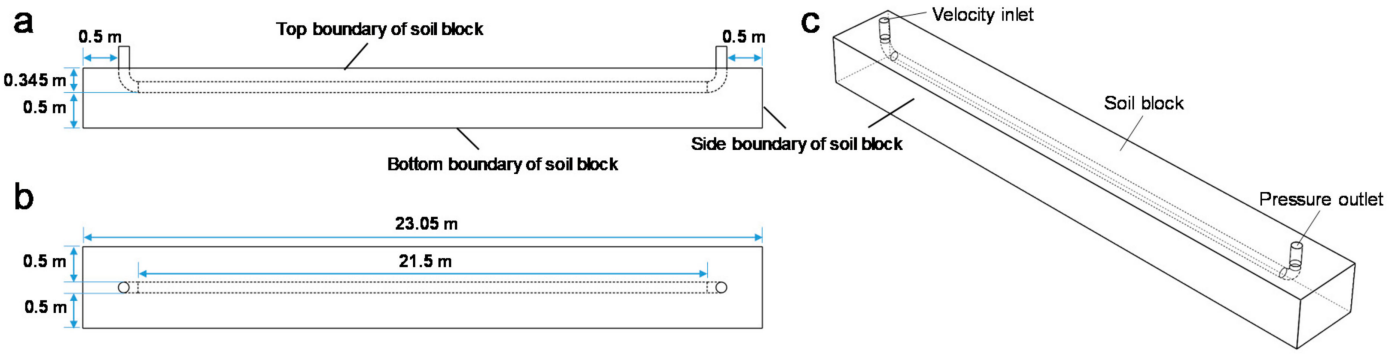

Figure 2. Schematic of the EAHE computational domain: (**a**) front view, (**b**) top view, and (**c**) perspective view.

Figure 3 shows the boundary conditions for the case used to validate the CFD model, which corresponds to 5 May 2019. The figure shows the variation of air temperature, relative humidity, and soil temperature at depths of 55, 140, 225, and 320 mm during the day. On the other hand, Figure 4 shows the soil block boundary conditions for the rest of the simulations that include representative days of the 9 months (March through November) where space cooling is required in Doha, Qatar. As shown in the figure, the soil temperature reaches its highest value in August. The inlet air temperature boundary conditions are shown along with the results of the simulations in Section 3.3. Given the fluctuating nature of ambient air relative humidity, the corresponding boundary conditions are not shown as a figure and are provided as Supplementary Materials.

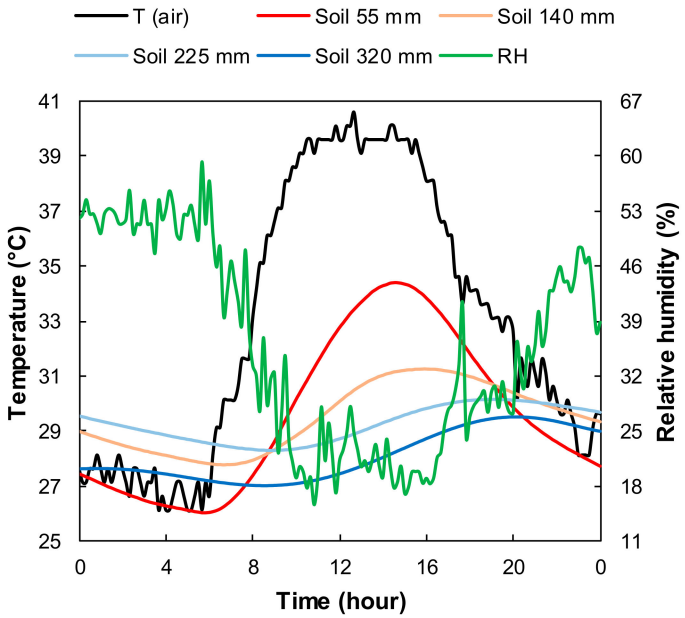

Figure 3. Boundary conditions for the validation of the CFD simulation. Experimental measurements of air temperature, relative humidity, and soil temperature on 5 May 2019. T = temperature, RH = relative humidity.

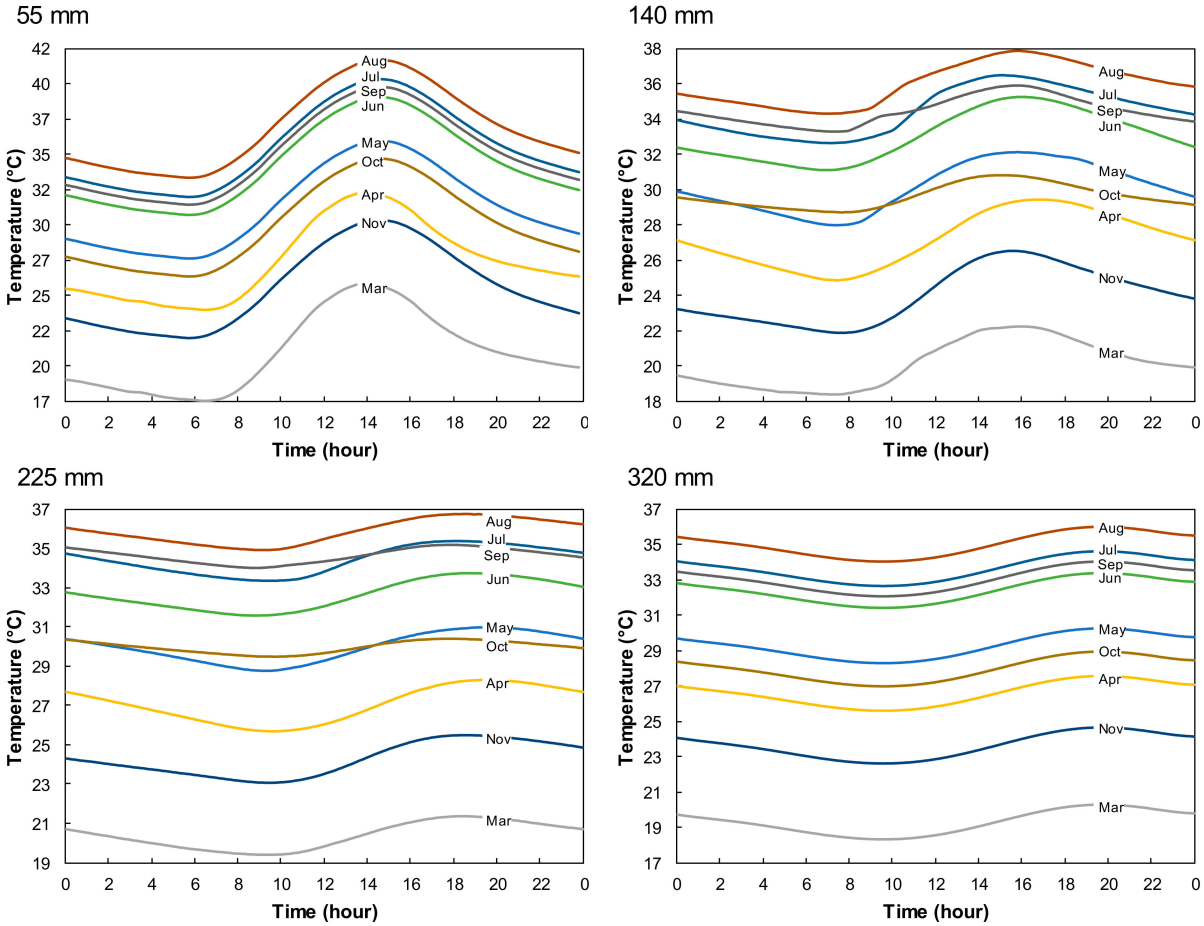

Figure 4. Soil temperature boundary conditions from March to November at depths of 55 mm (top surface), 140 mm, 225 mm, and 320 mm (bottom surface).

2.2.2. Grid Sensitivity

Figure 5a shows an isometric view of the computational grid, and Figure 5b shows a close-up view of the mesh near the inlet of the EAHE. The computational grid is a hybrid of a structured and an unstructured mesh. The EAHE mesh was created by extruding the face mesh shown in Figure 5b along the length of the tube. Smaller elements are used close to the wall of the EAHE to better capture the expected large variations of air temperature and velocity.

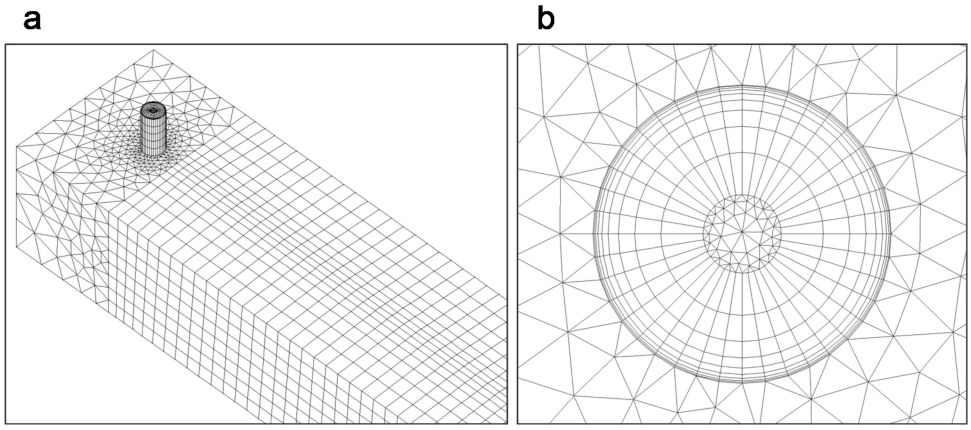

Figure 5. (**a**) Isometric view of the computational grid near the inlet of the EAHE. (**b**) Close-up view of the face mesh near the EAHE's inlet.

To ensure the grid independence of the simulation results, a grid sensitivity analysis was performed. By increasing the number of elements along the length of the tube and soil block and the perimeter of the tube diameter, a coarse grid of 157,404 elements was refined twice by a factor of about 2 to 323,879 elements (basic grid) and 645,151 elements (fine gird). The obtained outlet temperatures of the EAHE using the 3 girds during the day are shown in Figure 6. As shown in the figure, there is no significant difference between the 3 grid results, except for the prediction by the coarse grid at the peak of the plot, where lower temperatures are estimated compared with the other 2 grids. The maximum difference between the 3 grids is about 0.3% (0.1 °C). It was verified that the basic grid provided grid-independent results; therefore, it was used in performing the other simulations. The height of the wall-adjacent cells is about 0.5 mm, and y^+ is about 10.

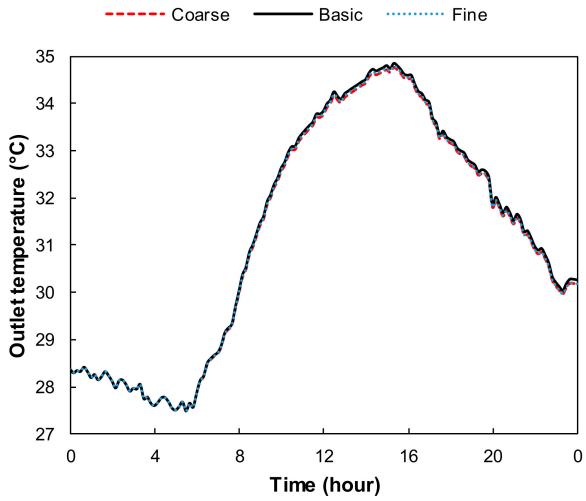

Figure 6. The CFD predicted outlet temperature of the EAHE during the day using the coarse, basic, and fine girds.

3. Results and Discussion

3.1. CFD Validation

To assess the validity of the CFD model, its predictions of the outlet temperature of the EAHE were compared with the measured outlet air temperatures on 5 May 2019. Figure 7 compares the predictions of the CFD model and the measurements of the EAHE outlet temperature during the day. The model predictions matched the measurements within the uncertainty of the measurements (±0.5 °C), which is indicated as a shaded band in the figure.

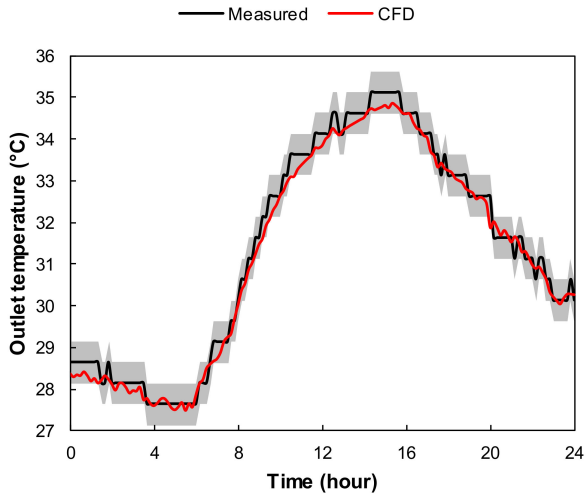

Figure 7. Comparison between measured and numerically predicted outlet temperature of the EAHE. The gray shading indicates the uncertainty of the measurements (±0.5 °C).

3.2. Weather Data

Figure 8 shows measured daily air temperature along the year in Doha, Qatar. During the year, the daily average air temperature ranges between 10.8 and 40.8 °C, the minimum daily air temperature ranges between 5.6 and 34.4 °C, and the maximum daily air temperature ranges between 13.4 and 48.9 °C. In this study, it is assumed that when the daily average air temperature is above 22 °C, space cooling in buildings is required. Therefore, as shown in the figure, during the three winter months of the year (December, January, and February) space cooling is not required. Therefore, the performance of the EAHE is simulated for the remaining 9 months of the year.

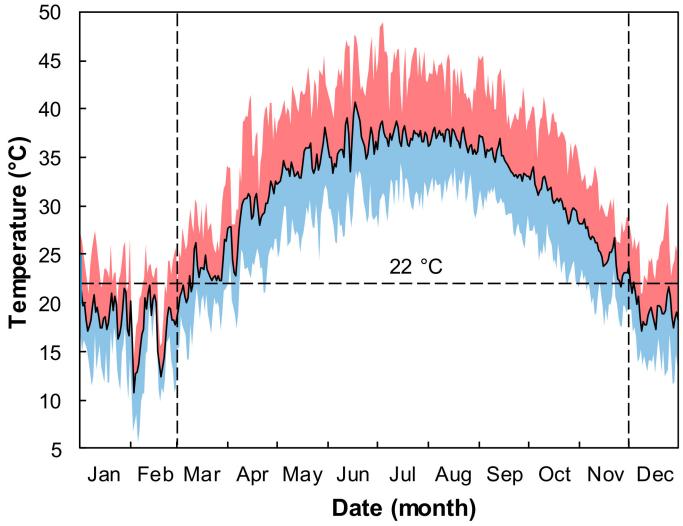

Figure 8. Measured daily air temperature in Doha, Qatar. The black line represents the average daily temperature, and the red and blue shaded areas are bounded by the maximum and minimum daily temperatures, respectively.

3.3. The Performance of the EAHE

Using the transient CFD model, the performance of the EAHE from March to November was modeled. The air flow rate (607 m^3/h) and length (21.5 m) of the EAHE corresponded to the experimental setup. The outlet temperature of the EAHE during typical days of March to November is shown in Figure 9. The highest maximum temperature difference between the inlet and outlet air occurs in April, with the outlet air temperature being approximately 8.5 °C below the inlet air temperature. The reason for this is the large difference between the ambient air and soil temperature. Even though the air temperature has increased significantly in April relative to March, the soil temperature due to its high thermal mass has not increased at the same rate. On the other hand, the smallest maximum temperature difference, which is approximately 3.3 °C, occurs in November. During the summer months (June to August), the highest daily temperature difference between the inlet and outlet air ranges between 5.2 and 6.8 °C.

Using the temperature change between the inlet air and outlet air (Figure 9), the cooling capacity of the EAHE during 9 months of the year is calculated using Equation (1). The cooling capacity of the EAHE during typical days of the spring months (March to May) is shown in Figure 10a. As shown in the figure, during these 3 months, the highest cooling capacity is obtained in April, reaching a maximum of 1700 W (0.5 tons of refrigeration), while the average cooling capacity during the day (operation hours) is approximately 690 W (0.2 tons of refrigeration). The daily average cooling capacity during May is approximately the same, 680 W, while during March, it is considerably lower, 359 W.

Figure 10b shows the cooling capacity during the day in the summer months (June to August). During this period, the maximum cooling capacity is about 1360 W, and the daily average cooling capacities during June, July, and August are 662, 509, and 547 W, respectively.

As shown in Figure 10c, during the fall (September, October, and November), the highest cooling capacity is 1212 W. The daily average cooling capacity is 540 W in September and 664 W in October, while the lowest is in November, 390 W. Overall, during these 9 months, the daily average cooling capacity of the EAHE is about 560 W (0.16 tons of refrigeration).

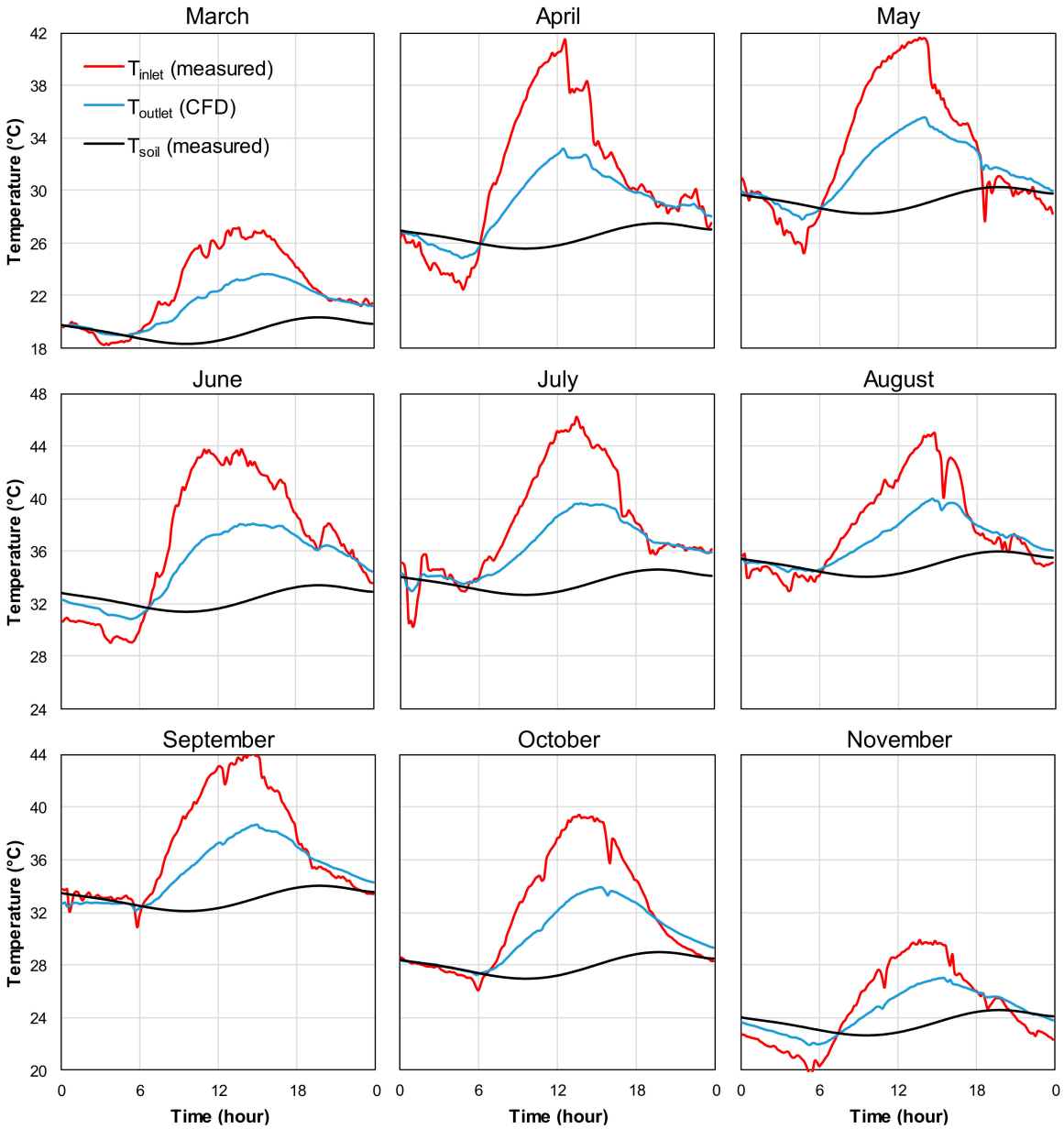

Figure 9. Predicted outlet temperature of the EAHE during typical days of March to November using experimentally measured ambient air temperature and soil temperature (320 mm deep).

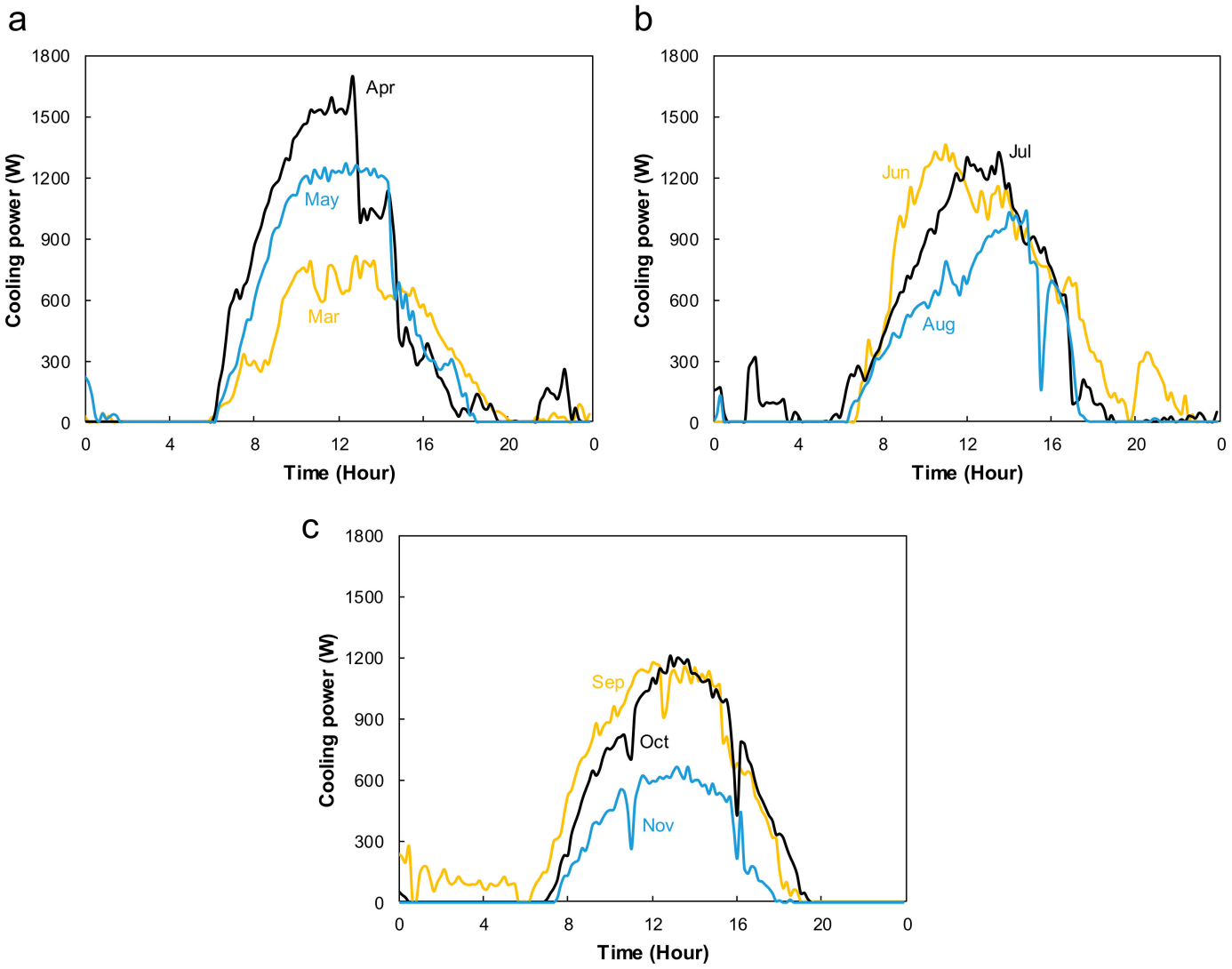

Figure 10. The calculated cooling capacity (W) of the EAHE during typical days of (**a**) March, April, and May; (**b**) June, July, and August; and (**c**) September, October, and November.

3.4. EAHE Energy Savings

In this section, a basic analysis is performed, in which it is assumed that the near-surface EAHE is used as a precooling system for a conventional air-conditioning system. The cooling capacity provided by the EAHE is calculated on an hourly basis using Equation (1), where measured ambient air temperature data are used as the inlet air temperature, and the CFD model is used to determine the outlet temperature of the EAHE over the period of 9 months, March through November.

By assuming that the conventional air conditioning system has a COP of 2, the required electricity by the conventional air conditioning system to provide the same amount of cooling power as the EAHE is calculated by dividing $P_{cooling}$ by a COP of 2. The electricity savings is then calculated by subtracting the fan power from the consumed power by the conventional air-conditioning system. Integrating the electricity savings over the operating time period of the EAHE gives the overall electricity savings.

The resulting electricity savings in kilowatt hour from using the EAHE to precool the air entering a conventional air-conditioning system is shown in Figure 11a on a monthly basis, which yields an annual electricity savings of 741 kWh. Over this period, the predicted average monthly electricity savings is 82 kWh, with a minimum of 31 kWh and a maximum of 115 kWh. Most of the electricity savings occurs during April to June, which

is approximately 44% of the total savings. On average, over the period of 9 months, the electricity consumption could be reduced by about 64% to provide the same cooling power using the near-surface EAHE compared with a conventional air-conditioning system.

The predicted daily hours of precooling provided by the EAHE from March to November is shown in Figure 11b. As shown in the figure, the EAHE operates between 10.8 and 18.5 h a day, with an average of 15.1 h a day. The operating hours of the EAHE are defined as the hours at which the soil temperature is lower than the ambient air temperature, that is, when the EAHE can provide cooling.

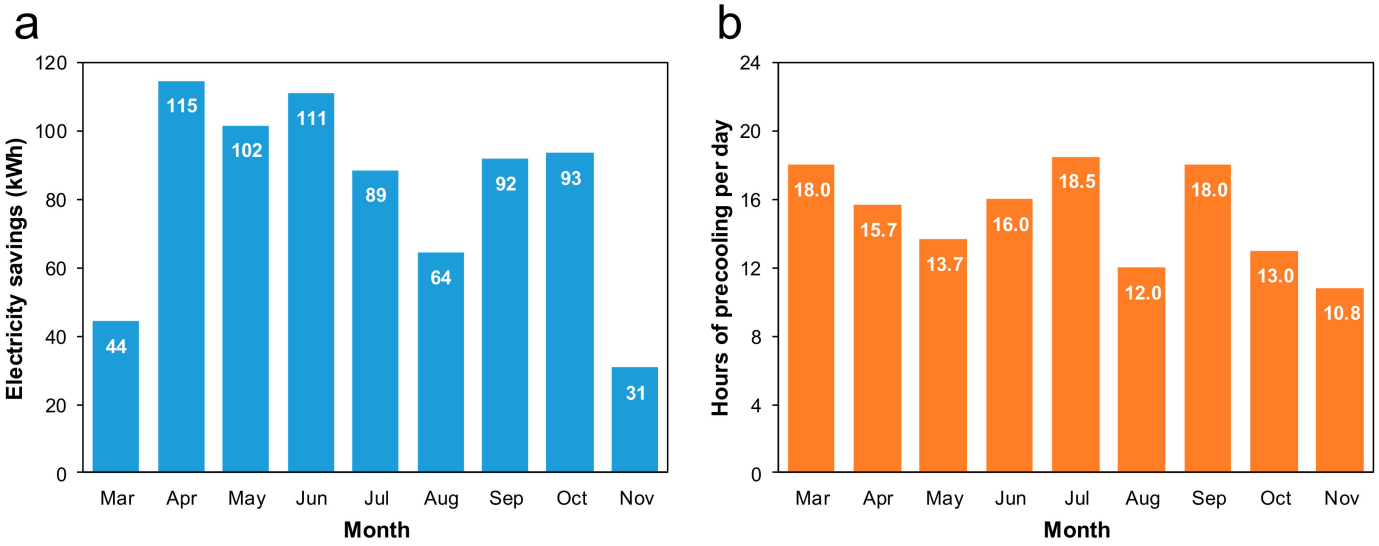

Figure 11. (**a**) Predicted electricity savings resulting from using the EAHE as a precooler. (**b**) Average daily operating hours of the EAHE.

3.5. CO_2 Emissions Reduction

All of Qatar's electricity is generated by natural gas, which is relatively cleaner than coal and fuel oil in terms of the emitted air pollutants. According to the most recent figures from the International Energy Agency [25], in 2018, the total electricity generated in Qatar was 47,913 GWh. The electricity consumed by the residential sector represented about 42.27% (20,252 GWh) of the total consumption. The total CO_2 emission was 86.99 megatons, of which approximately 26.44% (23 megatons) was due to electricity generation. Therefore, about 480 g of CO_2 is emitted per kWh of electricity generated. Considering annual energy savings of about 741 kWh of electricity, the use of the near-surface EAHE for precooling can avert 355.68 kg of CO_2 from being released into the atmosphere per year.

3.6. COP of EAHE

The average and maximum COP of the EAHE over the period of March to November is shown in Figure 12. The COP was calculated using Equation (2) ($P_{cooling}$ divided by P_{fan}). The average COP ranges between 3.6 and 6.9, while the maximum COP ranges between 6.3 and 17, which is considerably higher than that of a conventional air-conditioning system.

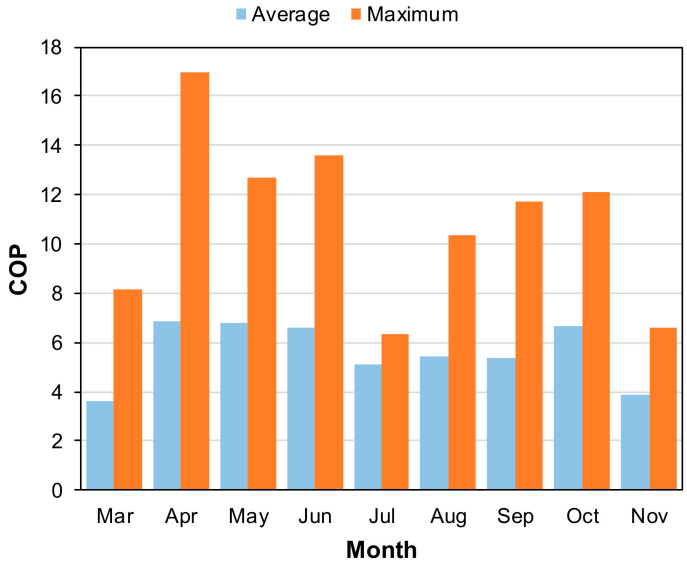

Figure 12. Predicted average and maximum COP of the EAHE during March to November.

3.7. Simple Payback Period

In order to determine the payback period of using the EAHE as a precooling unit, a simple financial analysis is performed. It is assumed that the EAHE is integrated into a building that has grass-covered ground; therefore, the cost of planting and maintaining the grass is not considered in the calculations.

For an electricity cost of USD 0.07/kWh, the cost savings of using the EAHE as a precooling unit will be about USD 51.87 per year. Given that the initial cost of the EAHE is about USD 130 (USD 55 for the fan, USD 50 for the tubes, and USD 25 for labor), the simple payback period of the EAHE is 2.5 years.

4. Conclusions and Summary

In this study, we quantified the energy savings resulting from using a near-surface EAHE with grass-covered ground as a precooling unit in hot desert climates. The outlet air conditions of the EAHE throughout March to November were predicted using a 3D transient CFD model. The main conclusions of this study are as follows:

- For an air flow rate of 607 m^3/h and a tube length of 21.5 m, the EAHE can cool ambient air temperature by as much as 8.5 °C.
- During August, where the soil temperature reaches its maximum value, the highest obtainable drop of ambient air temperature is about 5.2 °C.
- The highest daily average cooling capacity of the EAHE is 690 W, in April, while the lowest is 359 W, in March.
- The maximum cooling capacity of the EAHE is approximately 1700 W (0.5 tons of refrigeration).
- By using the EAHE as a precooling unit for a conventional air-conditioning system with a COP of 2, the highest monthly energy savings is 115 kWh, in April, and the lowest is 31 kWh, in November.
- The daily average COP of the EAHE ranges between 3.6 and 6.9, while the daily maximum COP ranges between 6.3 and 17.

Supplementary Materials: The following is available online at https://www.mdpi.com/article/10.3390/en14238044/s1, File S1: Relative Humidity Boundary Conditions.

Author Contributions: Conceptualization, A.P.; Data curation, A.P.; Formal analysis, A.P.; Funding acquisition, S.G.; Methodology, A.P.; Software, A.P.; Validation, A.P.; Visualization, A.P.; Writing—original draft, A.P.; Writing—review & editing, A.P. and S.G. All authors have read and agreed to the published version of the manuscript.

Funding: This work was supported by the Qatar National Research Fund under its National Priorities Research Program (grant number NPRP11S-0114-180295). The contents of this work are solely the responsibility of the authors and do not necessarily represent the official views of the Qatar National Research Fund.

Data Availability Statement: The data presented in this study are available as Supplementary Materials.

Acknowledgments: The authors acknowledge the Aspire Zone Foundation for providing technical support during the installation of the earth-to-air heat exchanger.

Conflicts of Interest: The authors declare no conflict of interest.

References

1. IEA. *World Energy Outlook 2018*; OECD: Paris, France, 2018. [CrossRef]
2. IEA. *The Future of Cooling*; OECD: Paris, France, 2018. [CrossRef]
3. Office of Energy Efficiency & Renewable Energy. *2011 Building Energy Data Book*; U.S. Department of Energy: Washington, DC, USA, 2011.
4. Bahadori, M.N. Passive Cooling Systems in Iranian Architecture. *Sci. Am.* **1978**, *238*, 144–154. [CrossRef]
5. Santamouris, M.; Ding, L.; Fiorito, F.; Oldfield, P.; Osmond, P.; Paolini, R.; Prasad, D.; Synnefa, A.J.S.E. Passive and active cooling for the outdoor built environment—Analysis and assessment of the cooling potential of mitigation technologies using performance data from 220 large scale projects. *Sol. Energy* **2017**, *154*, 14–33. [CrossRef]
6. Čermák, V.; Bodri, L.; Šafanda, J. Underground temperature fields and changing climate: Evidence from Cuba. *Palaeogeogr. Palaeoclimatol. Palaeoecol.* **1992**, *97*, 325–337. [CrossRef]
7. Goswami, D.Y.; Dhaliwal, A.S. Heat Transfer Analysis in Environmental Control Using an Underground Air Tunnel. *J. Sol. Energy Eng.* **1985**, *107*, 141–145. [CrossRef]
8. Bojic, M.; Trifunovic, N.; Papadakis, G.; Kyritsis, S. Numerical simulation, technical and economic evaluation of air-to-earth heat exchanger coupled to a building. *Energy* **1997**, *22*, 1151–1158. [CrossRef]
9. Wei, H.; Yang, D.; Guo, Y.; Chen, M. Coupling of earth-to-air heat exchangers and buoyancy for energy-efficient ventilation of buildings considering dynamic thermal behavior and cooling/heating capacity. *Energy* **2018**, *147*, 587–602. [CrossRef]
10. Wang, X.; Schmidt, B.; Zhang, G. Design-oriented modelling on cooling performance of the earth-air heat exchanger for livestock housing. *Comput. Electron. Agric.* **2018**, *152*, 51–58. [CrossRef]
11. Congedo, P.M.; Baglivo, C.; Bonuso, S.; D'Agostino, D. Numerical and experimental analysis of the energy performance of an air-source heat pump (ASHP) coupled with a horizontal earth-to-air heat exchanger (EAHX) in different climates. *Geothermics* **2020**, *87*, 101845. [CrossRef]
12. Zhou, T.; Xiao, Y.; Huang, H.; Lin, J. Numerical study on the cooling performance of a novel passive system: Cylindrical phase change material-assisted earth-air heat exchanger. *J. Clean. Prod.* **2020**, *245*, 118907. [CrossRef]
13. Vaz, J.; Sattler, M.A.; Brum, R.D.S.; Dos Santos, E.D.; Isoldi, L.A. An experimental study on the use of Earth-Air Heat. Exchangers (EAHE). *Energy Build.* **2014**, *72*, 122–131. [CrossRef]
14. Sakhri, N.; Menni, Y.; Ameur, H. Experimental investigation of the performance of earth-to-air heat exchangers in arid environments. *J. Arid. Environ.* **2020**, *180*, 104215. [CrossRef]
15. Hsu, C.Y.; Huang, P.C.; Liang, J.D.; Chiang, Y.C.; Chen, S.L. The in-situ experiment of earth-air heat exchanger for a cafeteria building in subtropical monsoon climate. *Renew. Energy* **2020**, *157*, 741–753. [CrossRef]
16. Díaz-Hernández, H.P.; Macias-Melo, E.V.; Aguilar-Castro, K.M.; Hernández-Pérez, I.; Xamán, J.; Serrano-Arellano, J.; López-Manrique, L.M. Experimental study of an earth to air heat exchanger (EAHE) for warm humid climatic conditions. *Geothermics* **2020**, *84*, 101741. [CrossRef]
17. Li, Y.; Long, T.; Bai, X.; Wang, L.; Li, W.; Liu, S.; Lu, J.; Cheng, Y.; Ye, K.; Huang, S. An experimental investigation on the passive ventilation and cooling performance of an integrated solar chimney and earth e air heat exchanger. *Renew. Energy* **2021**, *175*, 486–500. [CrossRef]
18. Wei, H.; Yang, D.; Du, J.; Guo, X. Field experiments on the effects of an earth-to-air heat exchanger on the indoor thermal environment in summer and winter for a typical hot-summer and cold-winter region. *Renew. Energy* **2021**, *167*, 530–541. [CrossRef]
19. Ozgener, O.; Ozgener, L.; Tester, J.W. A practical approach to predict soil temperature variations for geothermal (ground) heat exchangers applications. *Int. J. Heat. Mass. Transf.* **2013**, *62*, 473–480. [CrossRef]
20. Zheng, D.; Hunt, E.R.; Running, S.W. A daily soil temperature model based on air temperature and precipitation for continental applications. *Clim. Res.* **1993**, *2*, 183–191. [CrossRef]
21. Mihalakakou, G.; Santamouris, M.; Asimakopoulos, D.; Papanikolaou, N. Impact of ground cover on the efficiencies of earth-to-air heat exchangers. *Appl. Energy* **1994**, *48*, 19–32. [CrossRef]
22. Pakari, A.; Ghani, S. Performance evaluation of a near-surface earth-to-air heat exchanger with short-grass ground cover: An experimental study. *Energy Convers. Manag.* **2019**, *201*, 112163. [CrossRef]

23. Launder, B.E.; Spalding, D.B. The numerical computation of turbulent flows. *Comput. Methods Appl. Mech. Eng.* **1974**, *3*, 269–289. [CrossRef]
24. Pakari, A.; Ghani, S. Numerical evaluation of the thermal performance of a near-surface earth-to-air heat exchanger with short-grass ground cover: A parametric study. *Int. J. Refrig.* **2020**, *125*, 25–33. [CrossRef]
25. Int Energy Agency 2020. Key Energy Statistics. 2018. Available online: https://www.iea.org/countries/qatar (accessed on 24 November 2020).